Monte Carlo Simulations of Polyelectrolytes at Charged Micelles. 3. Effects of Surfactant Tail Length

Torsten Wallin* and Per Linse

Physical Chemistry 1, Center for Chemistry and Chemical Engineering, Lund University, P.O. Box 124, S-221 00 Lund, Sweden

Received: January 16, 1997; In Final Form: April 23, 1997[⊗]

The complexation of a charged micelle and an oppositely charged polyelectrolyte was studied by the use of a simple model system. The size of the micelle was varied to correspond to the change in surfactant tail length of real cationic surfactants, and the surface charge density of the micelle was kept constant. Structural data of the micelle−polyelectrolyte complex and thermodynamic quantities of the complexation as a function of the micellar aggregation number were obtained by the use of the Monte Carlo simulation technique and thermodynamic integration. The ratio of the critical aggregation concentration, cac, and the critical micellization concentration, cmc, was calculated, cac being the lowest surfactant concentration at which the surfactants self-assemble in the presence of polyelectrolyte. The cac was found to be ca. 15 (for smaller micelles formed by C_8TA^+ surfactants) to ca. 75 (for larger micelles formed by $C_{12}TA^+$ surfactants) times smaller than the corresponding cmc values. This decrease in the cac/cmc ratio at increasing aggregation numbers agrees well with experimental data from solutions of alkyltrimethylammonium bromide and charged polysaccharides.

Introduction

An increasing number of aqueous mixtures of polyelectrolytes and charged surfactants have been investigated during recent years.[1−19] One distinctive character observed for those mixtures is the large difference in the cmc and the cac.[12−17] The cmc (critical micellization concentration) and the cac (critical aggregation concentration) are the lowest concentrations at which micelles are formed without and with polyelectrolyte present in the solution, respectively. It has been shown that an increase in the surfactant chain length of alkyltrimethylammonium bromide (C_nTAB) makes the cac/cmc ratio to decrease; i.e., the cac reduces faster than the reduction of the cmc at increasing surfactant chain length.[12,13]

We have previously investigated the surfactant−polyelectrolyte complexation in dilute solutions by examining the interaction between a micelle and an oppositely charged polyelectrolyte using a simple model system. The micelle is treated as a hard charged sphere and the polyelectrolyte as a chain of charged beads connected with harmonic bonds. The reported results from our previous studies (parts 1 and 2)[18,19] showed that the micelle−polyelectrolyte complexation leads to (i) a strong reduction of the electrostatic energy of the system and (ii) a release of counterions of the micelle and polyelectrolyte. Both phenomena are important for the difference between the cmc and the cac, and the phenomena become less prominent as the polyelectrolyte becomes stiffer (part 1) and as the polyelectrolyte linear charge density is reduced (part 2). Hence, the cac, which could to be up to 2 orders of magnitude lower than the cmc, increases with increasing chain rigidity and decreasing linear charge density of the polyelectrolyte. The aim of this third study is to investigate how the predicted cac/cmc ratios depend on micellar properties. In particular, the model systems were designed to be comparable to experimental measurements involving C_nTAB surfactants. The variation of the surfactant tail length is modeled by using micelles of different sizes at constant surface charge density, and we examine how the micelle−polyelectrolyte complex structure and the cac/cmc ratio depend on the micellar size.

[⊗] Abstract published in *Advance ACS Abstracts,* June 1, 1997.

The remainder of the paper is organized as follows. In the next section, we recapitulate the main parts of the method and model system employed. First, we relate the cac/cmc ratio to the free energy of complexation between a micelle and a polyelectrolyte in dilute solution, and thereafter we describe the model system used. Furthermore, we account for the free energy evaluation path employed and give some aspects of the Monte Carlo simulations. In the following section, structural and thermodynamic results of the complexation are presented and discussed. We also present calculated cac/cmc ratios, discuss some approximations involved in the investigation, and relate the cac/cmc ratios of the model system to experimental data. In the last section, we give our main conclusion.

Method and Model System

The method and model system are the same as in part 1. We will therefore only give a brief description of our assumptions and the protocol used.

Background. The addition of a polyelectrolyte to a solution of oppositely charged surfactants facilitates the micelle formation of the surfactants. We express the factor with which the cmc is reduced by upon the addition of the polyelectrolyte by[18,20]

$$\frac{\text{cac}}{\text{cmc}} = \exp\left[\frac{\Delta A_{\text{pe}}}{N_{\text{agg}} RT}\right] \tag{1}$$

where ΔA_{pe} is the change in free energy of the complexation between one micelle with concomitant counterions and one polyelectrolyte with its counterions. In eq 1, N_{agg} is the micellar aggregation number, R the gas constant, and T the absolute temperature. Furthermore, we assume that the aggregation number is not affected by the presence of the polyelectrolyte and that we can neglect the volume−pressure work caused by the addition of polyelectrolyte and thereby identify the Gibbs free energy with the corresponding Helmholtz free energy.

Model System. The specification of a simple model system, containing what we hope are all the essential aspects of the real system, makes it possible to calculate ΔA_{pe}, in principle, exactly. The main simplifications of the model systems are as

S1089-5647(97)00224-1 CCC: $14.00

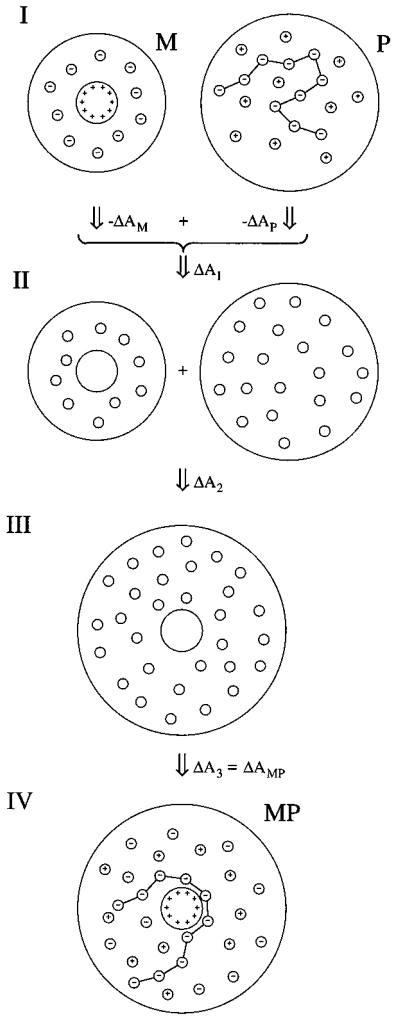

Figure 1. Illustration of the initial micellar (M) and polyelectrolyte (P) systems (state I), the final mixed micelle−polyelectrolyte (MP) system (state IV), and the two intermediate and decoupled systems (states II and III). The pathway for the calculation of the Helmholtz free energy of mixing, ΔA_{pe}, is also indicated (see text for details).

follows: (i) The primitive model is used; i.e., the water is treated as a dielectric medium and enters the model only through its dielectric permittivity, and all other constituents are described in terms of hard spheres with point charges in the centers of the spheres. (ii) The cell model is applied; one micelle and/or one short polyelectrolyte plus counterions are enclosed in a spherical cell. (iii) The concentration of free surfactant is neglected. (iv) The polyelectrolyte is modeled as a chain of charged hard spheres (beads) joined by harmonic bonds with the flexibility controlled by harmonic angular energy terms. (v) The micelle is described as a hard sphere with fixed charge and radius, and hence the aggregation number is assumed not to change upon addition of the polyelectrolyte.

Figure 1 illustrates the cell model of the initially separated micellar (M) and polyelectrolyte (P) solutions, the final mixed micelle−polyelectrolyte (MP) solution, and two decoupled intermediate states (further described below). The radii of the cells are selected to yield the same concentrations of ions and polyelectrolyte as in part 2. The P and MP cells can accommodate a nearly fully stretched polyelectrolyte. The volume is conserved upon mixing.

The M and MP systems contain one micelle with fixed position in the center of the cell and freely moving monovalent counterions, and the P and MP systems contain one polyelectrolyte with n_{bead} beads and its counterions. In the P system, the position of one central bead of the chain is fixed at the center of the cell, whereas in the MP system, the same bead is fixed at the surface of the micelle. In the former case, the constraint keeps the polyelectrolyte in the center of the cell and hence minimizes the effect of the cell boundary. In the latter case the constraint enforces the polyelectrolyte to be close to the micelle. A separation would imply a disassembling of the micelle (since the surfactant concentration is below the cmc) with an accompanied high free energy penalty. Our constraint formally corresponds to an infinitely large cost of disassembling the micelle.

TABLE 1: Data of the Sizes and Charges of the Three Simulated Micelles[a]

n_c	l_{max} (Å)	$N_{agg,c}$	area/$N_{agg,c}$ (Å^2)	R_{mic} (Å)	N_{agg}	area/N_{agg} (Å^2)
8	11.62	27	62.4	15.0	30	94.3
10	14.15	40	62.8	17.5	41	93.9
12	16.68	56	63.6	20.0	53	94.8

[a] The hydrocarbon chain lengths l_{max} are evaluated according to $l_{max} = 1.500 + 1.265n_c$, where n_c is the number of carbons, and the hydrocarbon tail aggregation numbers $N_{agg,c}$ according to $N_{agg,c} = V_{agg}/V_c$, where $V_{agg} = {}^4/_3\,\pi l_{max}^3$ and $V_c = 27.4 + 26.9n_c$.[24] The C_nTAB lengths R_{mic} are evaluated according to $R_{mic} = l_{head} + l_{max}$, where l_{head} is estimated to 3.36 Å. The final micellar aggregation numbers N_{agg} are slightly altered to keep the micellar surface charge density constant.

The total energy of a system (M, P, or MP) can be written as a sum of nonbonded, bonded, and angular energy terms. The nonbonded energy is given by the Coulomb interactions and hard-sphere overlap repulsion among the charged hard spheres. The dielectric permittivity is constant throughout the system, and hence surface polarization is neglected.[23] The total bond energy between adjacent beads in the chain is expressed as a sum of harmonic spring terms with an equilibrium distance between adjacent beads $r_0 = 8$ Å, a force constant $k_{bond} = 0.2$ N m^{-1}, and a factor that facilitates the thermodynamic integration (see part 1 for further details). The total angular energy, controlling the flexibility of the polymer backbone, is written as a sum of harmonic angular energy terms with an equilibrium angle $\alpha_0 = 180°$ and a force constant $k_{ang} = 3.74 \times 10^{-24}$ J/deg^2.

The complexation has been investigated for three different micelles. The micellar charge and size were determined from (i) the packing constraint of octyl, decyl, and dodecyl chains and (ii) the size of the headgroup of the C_nTA^+ surfactants. The final aggregation numbers were slightly modified to achieve a constant surface charge density (cf. Table 1 for further details). The finally adjusted micellar aggregation numbers (30, 41, and 53) still correspond well to what is expected for C_8TA^+ micelles and found for $C_{10}TA^+$ and $C_{12}TA^+$ micelles.[25,26] The corresponding micellar radii are 15, 17.5, and 20 Å, respectively. The three micellar systems will in the following be referred to as s (small), m (medium), and l (large) and the different micelles by their aggregation number.

The properties of the M, P, and MP systems and their constituents are shown in Table 2. The surfactant and bead concentrations in the M and P systems, respectively, are the same as in part 2, but the number of polyelectrolyte charges per micelle charge has been reduced from 2 to 1.5 charged beads per surfactant charge for computational reasons, yielding a somewhat higher surfactant and surfactant counterion concentration in the MP systems than in the MP system of part 2.

Calculation of Helmholtz Free Energy. Beside the initial and final systems described above (state I and IV), Figure 1 shows the two intermediate states. These are related to state I and IV, respectively, but the interactions are decoupled except for the hard-sphere repulsion. By using the four states, ΔA_{pe} for the mixing of the M and P systems to obtain the MP system is expressed as the sum of three terms named ΔA_1, ΔA_2, and

TABLE 2: Data of the Simulated Systems

		small	medium	large
cell radius, M system (Å)	$R_{cell,M}$	91.0	101.0	110.0
cell radius, P system (Å)	$R_{cell,P}$	273.1	303.9	330.8
cell radius, MP system (Å)	$R_{cell,MP}$	276.4	307.6	334.9
micelle radius (Å)	R_{mic}	15.0	17.5	20.0
bead radius (Å)	R_{bead}	2.0	2.0	2.0
small ion radius (Å)	R_{ion}	2.0	2.0	2.0
micelle charge (e)	z_{mic}	30	41	53
bead charge (e)	z_{bead}	−1	−1	−1
small ion charge (e)	z_{ion}	±1	±1	±1
micelle surface charge density (e/Å$^2 \times 10^2$)	σ_{mic}	1.061	1.065	1.054
no. of beads	n_{bead}	45	62	80
no. of cations	n_{cation}	45	62	80
no. of anions	n_{anion}	30	41	53
temperature (K)	T	298		
relative dielectric permittivity	ϵ_r	78.3		

ΔA_3, where $\Delta A_1 = -\Delta A_M - \Delta A_P$ and $\Delta A_3 = \Delta A_{MP}$. The quantities ΔA_M, ΔA_P, and ΔA_{MP} denote the free energy differences between the coupled and decoupled M, P, and MP systems, respectively. The free energy contributions from the first and last step, ΔA_1 and ΔA_3, respectively, are obtained from Monte Carlo simulations and thermodynamic integration, whereas ΔA_2 is calculated from analytic theory.

The calculations of ΔA_M, ΔA_P, and ΔA_{MP} are performed by introducing a coupling parameter λ that continuously brings the decoupled systems into the interacting ones as λ varies from 0 to 1. The free energy difference between the states described by $\lambda = 0$ and $\lambda = 1$ is then given by

$$\Delta A \equiv A(1) - A(0) \equiv \int_0^1 \frac{\partial}{\partial\lambda} A(\lambda)\, d\lambda = \int_0^1 \left\langle \frac{\partial}{\partial\lambda} U(\lambda) \right\rangle d\lambda \quad (2)$$

where $\langle ... \rangle$ denotes a canonical ensemble average. The integral is discretisized by a summation using the trapezoidal rule, and up to 16 terms are used.

The free energy of mixing the two hard-sphere systems to a single one, ΔA_2, is obtained by the integration of the Carnahan−Starling compressibility along an isotherm.[21,22] The choice of additive cell volumes and not too dissimilar particle concentrations make ΔA_2 small, $0.25RT$ for the mixing, which is negligible compared with ΔA_1 and ΔA_3.

Monte Carlo Simulation. We performed Monte Carlo simulations according to the Metropolis algorithm[27] on the M, P, and MP systems to obtain structural information of the fully coupled systems and to evaluate the ensemble averages as described above. The convergence was enhanced by using the Pivot algorithm[28] and by weighting the number of trial moves to the benefit for the polyelectrolyte beads. (The polyelectrolyte beads were selected ca. 3 times as often as the other moving constituents.) After the equilibration, in general 5×10^6 trial moves per particle (polyelectrolyte beads and small ions) were generated for the sampling. The number of trial moves was twice as large for the P and MP systems at $\lambda = 0.9-1.0$, whereas for $\lambda = 0.25-0.325$ the number of trial moves per particle was reduced to $1.5 \times 10^6-4 \times 10^6$. For $\lambda = 0.1-0.2$ and for the M systems the simulation length was decreased to 1×10^6 trial moves per particle.

The reported uncertainty of simulated quantities is one standard deviation of their means and is estimated from the spread among the means of subbatches of the total number of MC steps. The smallest $\sigma(\Delta A)$ is obtained for $\Delta A_{M,s}$ ($0.01RT$) and the largest for $\Delta A_{P,l}$ ($0.24RT$), whereas the variance σ^2 of ΔA_{pe} is estimated from $\sigma^2(\Delta A_{pe}) = \sigma^2(\Delta A_M) + \sigma^2(\Delta A_P) + \sigma^2(\Delta A_{MP})$.

The simulations were performed on IBM RS/6000 390, or equivalent, workstations and involved altogether nearly 10 000 CPU hours.

Results and Discussion

Polyelectrolyte Structure. P and MP Systems. Table 3 displays the calculated properties of the 45−80 bead long polyelectrolyte without (P systems) and with the micelle present (MP systems). Regarding the P systems, the average and root-mean-square bead−bead separation increases slightly as the number of polyelectrolyte beads increases from 45 to 80 due to increasing electrostatic repulsion among the charged beads in the chain. Similarly, the persistence length and, in particular, the statistic Kuhn segment length show an increase as the polyelectrolyte becomes longer. Still, the ratio $\langle R_{ee}^2 \rangle / \langle R_G^2 \rangle$ is essentially constant (9.2−9.4) for the different number of beads. Thus, the polyelectrolyte appears not to change its overall shape in the investigated interval, but the local stiffness increases slightly with the increasing number of beads.

A comparison between the P and MP systems shows that the bead−bead separation is shortened by ca. 0.3 Å when the polyelectrolyte is complexed with the micelle. The root-mean-square end-to-end distance are reduced by a factor of ca. 4 and the radius of gyration by a factor of 3−4. The ratio $\langle R_{ee}^2 \rangle / \langle R_G^2 \rangle$ is decreased from 9.2 to 9.4 for the P systems to 6.2, 5.8, and 8.9 for the MP systems with $N_{agg} = 30$, 41, and 53, respectively. Thus, whereas the free polyelectrolyte with its counterions is more extended than a Gaussian coil, the $\langle R_{ee}^2 \rangle / \langle R_G^2 \rangle$ ratio becomes close to 6 when the polyelectrolytes with $n_{bead} = 45$ and 62 are complexed with the micelle with $N_{agg} = 30$ and 41, respectively, while the change in the extension upon complexation becomes much smaller for the longest polyelectrolyte and largest micelle. An increase in $\langle R_{ee}^2 \rangle / \langle R_G^2 \rangle$ with increasing n_{bead} and N_{agg} for the complexed polyelectrolyte is, however, expected. As shown below, a part of the polyelectrolyte is wrapped around the micelle, whereas the remaining part is stretched away from the micelle. For geometrical reasons, the linear dimension of the latter part increases faster than that of the former one at increasing n_{bead} and N_{agg}. Hence, the polyelectrolyte as a whole becomes more extended as n_{bead} and N_{agg} are increased simultaneously. This is also reflected in the change of the statistical Kuhn segment length.

Intermolecular Structure. M and MP Systems. The structures of the M and MP systems have further been investigated by calculation of radial distribution functions, $g(r)$, of the negatively charged polyelectrolyte beads, of the anions, and of the cations with respect to the center of the micelle. Figure 2a shows that in the absence of polyelectrolyte, the counterions of the micelle are strongly accumulated close to the micellar surface. By integration of the $g(r)$, we obtain 33, 41, and 45% of the counterions in the volume within 5 Å from the distance of closest approach ($R_{contact} = R_{mic} + R_{ion} =$ 17, 19.5, and 22 Å) for $N_{agg} = 30$, 41, and 53 Å, respectively. As anticipated, the accumulation becomes stronger as the curvature decreases at constant surface charge density.

In the presence of the polyelectrolyte, the counterions of the micelle are replaced by the charged polyelectrolyte beads which are even stronger accumulated in the neighborhood of the micellar surface (Figure 2b). Also here the accumulation is enhanced as N_{agg} is increased and by analogy with the case of only small counterions. Again considering the volume between $R_{contact}$ and $R_{contact} + 5$ Å, we find polyelectrolyte beads corresponding to 87, 90, and 93% of the micellar charge for $N_{agg} = 30$, 41, and 53, respectively. A comparison with the corresponding numbers given above for the counterions in the absence of the polyelectrolyte shows the much larger efficiency

TABLE 3: Average Angle between Consecutive Segments ($\langle\alpha\rangle$), Average Bead−Bead Separation ($\langle l_{bb}\rangle$), Average Root-Mean-Square Bead−Bead Separation ($\langle l_{bb}^2\rangle^{1/2}$), Statistical Kuhn Segment Length (l_K), Persistence Length (l_P), Radius of Gyration ($\langle R_G^2\rangle^{1/2}$), and Root-Mean-Square End-to-End Distance ($\langle R_{ee}^2\rangle^{1/2}$) of the Polyelectrolyte for the Angle Force Constant $k_{ang} = 3.74 \times 10^{-24}$ J/deg^2 and Equilibrium Bead−Bead Separation $r_0 = 8$ Å of the P and MP Systems[a]

system	$\langle\alpha\rangle$ (deg)	$\langle l_{bb}\rangle$ (Å)	$\langle l_{bb}^2\rangle^{1/2}$ (Å)	l_K (Å)	l_p (Å)	$\langle R_G^2\rangle^{1/2}$ (Å)	$\langle R_{ee}^2\rangle^{1/2}$ (Å)	$\langle R_{ee}^2\rangle/\langle R_G^2\rangle$
P_s	150.9	8.508	8.565	189	57.1	87	266	9.3
P_m	150.9	8.520	8.577	246	60.0	117	358	9.4
P_l	151.0	8.528	8.585	295	62.5	147	446	9.2
MP_s	143.4	8.189	8.248	14	37.9	28	70	6.2
MP_m	144.3	8.212	8.271	13	40.9	33	79	5.8
MP_l	145.1	8.217	8.277	22	43.3	40	119	8.9

[a] $\langle\alpha\rangle$, $\langle l_{bb}\rangle$, and $\langle l_{bb}^2\rangle$ are averaged over all angles and all bond distances, respectively, of the polyelectrolyte. l_K is evaluated according to $l_K = \langle R_{ee}^2\rangle/\langle L\rangle$, where $\langle L\rangle$ is the average polymer contour length, and l_P according to $l_P = (\langle l_{bb}^2\rangle^{1/2}/2)(C_N + 1)$, where $C_N = (1 + \gamma)/(1 - \gamma) - (2\gamma/N)[(1 - \gamma^-)/(1 - \gamma)^2]$ and $\gamma = \cos(\pi - \langle\alpha\rangle)$.[31] Largest estimated uncertainties are $\sigma(\langle\alpha\rangle) = 0.1°$, $\sigma(\langle l_{bb}^2\rangle^{1/2}) = 1 \times 10^{-4}$ Å, $\sigma(l_K) = 1$ Å, $\sigma(l_P) = 0.1$ Å, $\sigma(\langle R_G^2\rangle^{1/2}) = 0.4$ Å, and $\sigma(\langle R_{ee}^2\rangle^{1/2}) = 2$ Å.

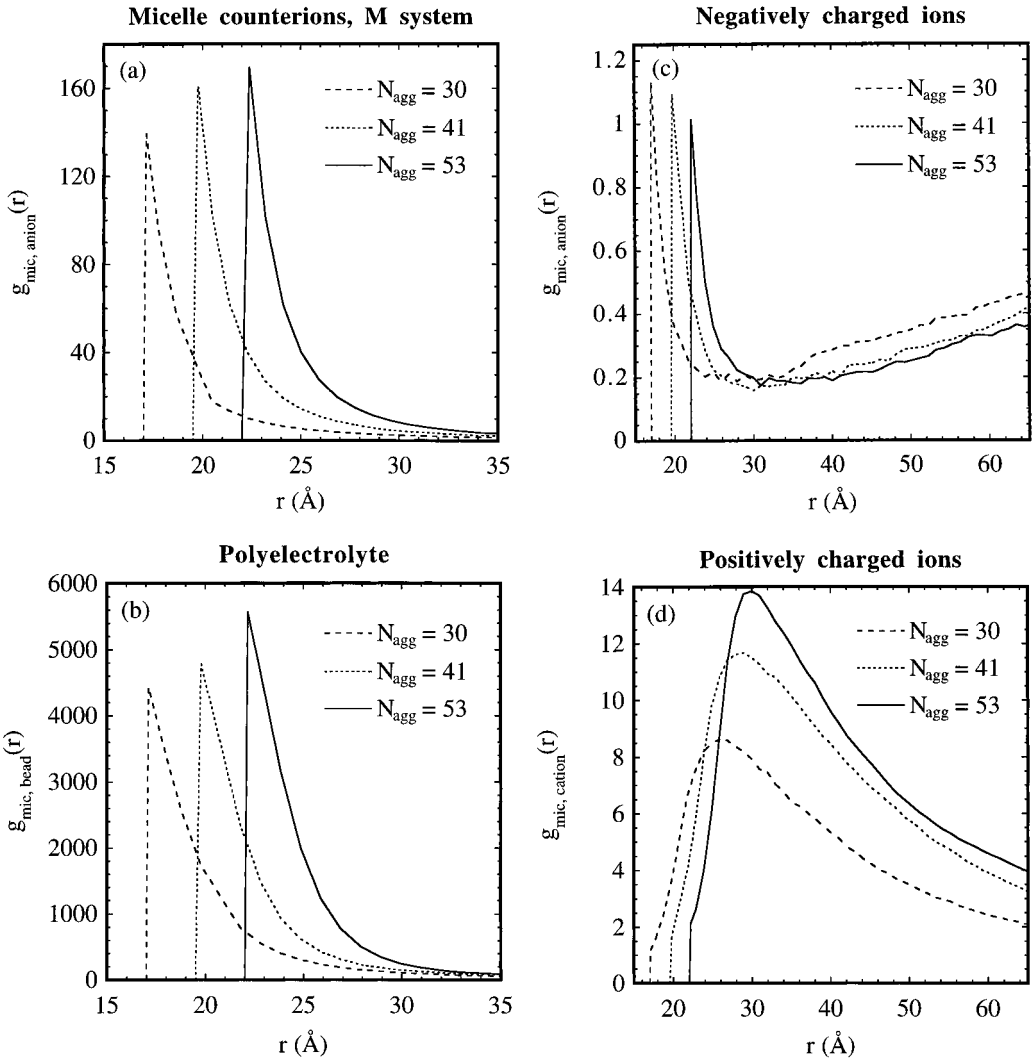

Figure 2. (a) Micelle−anion radial distribution function for the M system and (b) micelle−polyelectrolyte bead, (c) micelle−anion, and (d) micelle−cation radial distribution functions for the MP system ($g_{mic,i}(r)$) versus the separation (r) at indicated micellar aggregation numbers (N_{agg}). Since there is only one micelle and it is fixed, the local concentration of particle i is given by $\rho_i(r) = \rho_i g_{mic,i}(r)$, where ρ_i is the average number density of particle i in the system. In (b) the δ-contribution from the polyelectrolyte bead fixed at $r = 17$, 19.5, and 22 Å, respectively, is not displayed.

of the polyelectrolyte to shield the charges of the micelle. The thicknesses of the adsorbed polyelectrolyte layers (say, $g_{mic,bead} > 1000$ corresponding to a local bead number density $\rho > 5 \times 10^{-4}$ Å^{-3}) are nearly the same for all micelle sizes.

Figure 2c shows the distributions of the anions (counterions to the micelle) at different N_{agg}. We obtain $g_{mic,anion}(r) < 1$ in the vicinity of the micelle; i.e., these anions are depleted from the neighborhood of the micelle by the strong accumulation of the polyelectrolyte. However, the radial distribution function still displays a local maximum at micellar contact and a global minimum occurs ca. 10 Å from the distance of closest approach.[18] The contact values are slightly greater than one and decreases somewhat with increasing N_{agg}, and the local minimum is slightly moved away from the micellar surface as N_{agg} increases. These observations are in line with the fact that the polyelectrolyte is more tightly complexed with the micelle as N_{agg} increases.

Also the distribution of the cations (counterions of the polyelectrolyte) depends on the micellar curvature. Figure 2d shows that there is a pronounced maximum in the local concentration at $r_{max} - R_{contact} = 8-11$ Å outside the distance of closest approach. As N_{agg} is increased from 30 to 53, the

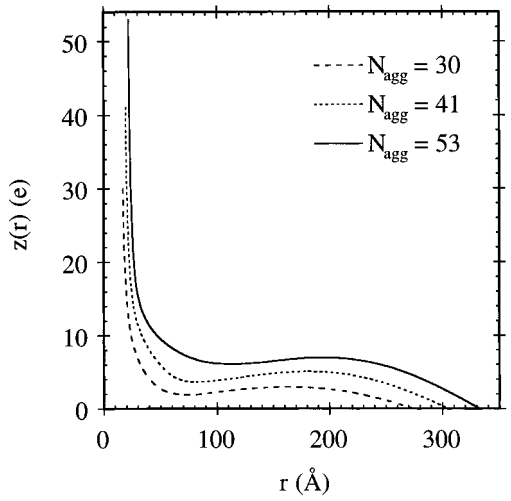

Figure 3. Integrated net charge ($z(r)$) for the MP system versus the separation (r) at indicated micellar aggregation numbers (N_{agg}).

local concentration increases and the maximum comes closer to the micelle surface, i.e., $r_{max} - R_{contact}$ decreases. This increase in the cation concentration occurs as a consequence of the increase in the local concentration of the polyelectrolyte beads close to the micelle. Also, the reduction of $r_{max} - R_{contact}$ is in line with the fact that parts of the polyelectrolyte become more tightly bound to the micelle as the micellar curvature decreases at constant surface charge density.

Thus, the effect of increasing the surfactant tail length is that the adsorbed polyelectrolyte layer as well as the micellar coion layer around the micelle becomes more prominent, and the micelle counterions become more depleted from the neighborhood of the micelle.

The radially integrated number of elementary charges for the three MP systems are shown in Figure 3. The limiting values are $z(R_{contact}) = N_{agg}$ and $z(R_{cell}) = 0$. Close to the micellar surface ($30 \le r_0 \le 50$ Å) $z(r)$ drops to ca. 15% of its maximum value due to the strong polyelectrolyte accumulation. After a weak minimum ca. 50−90 Å outside the micellar surface, the integrated number of charges stays approximately constant and decreases gradually to zero close to the cell boundary. Thus, in these systems the polyelectrolyte strongly screens the charges of the micelles, as concluded above, but no charge reversal appears when including the small ions as well.

Finally, Figure 4 shows snapshots of the micelle−polyelectrolyte complex at $N_{agg} = 30$, 41, and 53, respectively. These pictures illustrate graphically how the aggregation number of the micelle and the length of the polyelectrolyte affect the structural behavior of the micelle−polyelectrolyte complex, and the images partly visualize the results discussed above.

The picture that emerges is thus that the polyelectrolyte makes a firm complex with the charged micelle (cf. Figure 2b and Figure 4), and ca. 90% of the micellar charge is screened by the polyelectrolyte charges located within 5 Å from the distance of closest approach. Although the net charge of the whole micelle−polyelectrolyte complex is opposite that of the micelle (remember that $n_{bead} = 1.5N_{agg}$), there is no integrated charge reversal due to the screening by the cations which form a diffuse layer which partly overlaps the outer part of the adsorbed polyelectrolyte layer. In all of the MP systems the persistence length l_P is close to $l_P^* = S_{eff}/4 \approx 27$, 31, and 35 Å, where $S_{eff} = 2\pi(R_{mic} + R_{bead})$ is the effective circumference of the layer where the polyelectrolytes closest to the micelle reside. (The persistence length for the polyelectrolyte in the MP system given in Table 3 is averaged over the whole chain. Since l_P is larger for the nonadsorbed part, l_P for the adsorbed part is smaller than the values given in Table 3.) Thus, the polyelectrolyte is flexible enough to fold itself around the micelle, as also illustrated in Figure 4. A comparison with l_P for the P system shows that the persistence length of the adsorbing part in the MP system is reduced by ca. 50% upon the complexation.

Thermodynamics. We will now deal with changes in energy, entropy, and free energies for the coupling process of the M, P, and MP systems separately and then consider the corresponding quantities for the overall mixing process as described in Figure 1. We recall that the contribution from step 2 is negligible.

The obtained differences in the thermodynamic quantities between the coupled and decoupled systems can be seen in Figure 5. Figure 5a shows the corresponding differences in energy for the M, P (dashed curves), and MP (solid curves) systems as a function of N_{agg}. Included is also the division of ΔU into contributions from the nonbonded (i.e., electrostatic), the bonded, and the angular energy terms. The corresponding

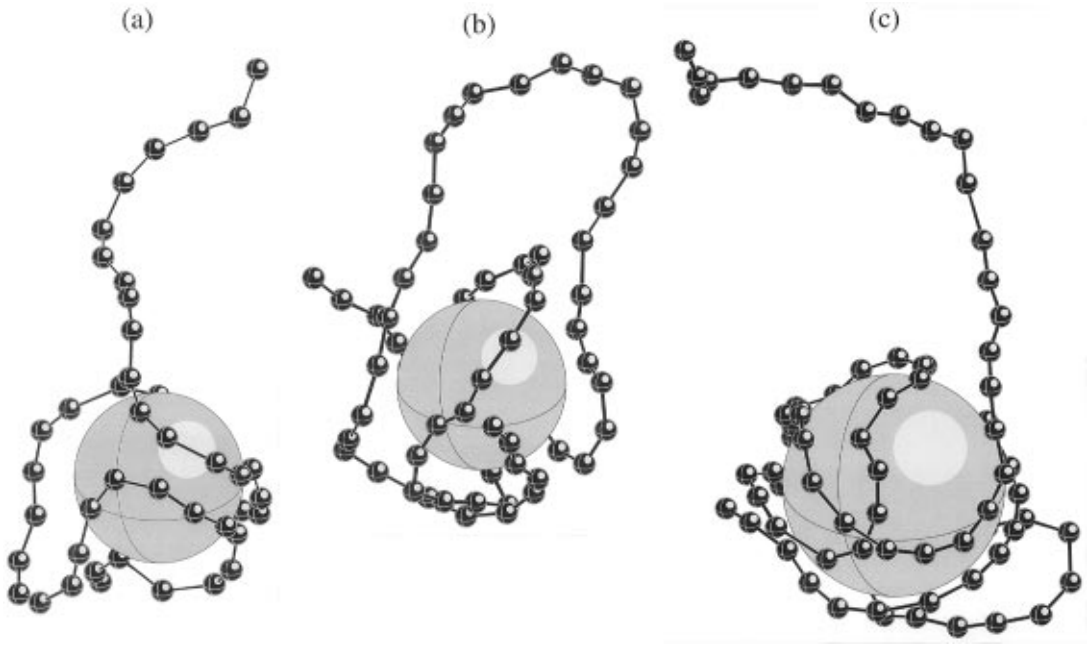

Figure 4. Images of the micelle and the polyelectrolyte for the MP system at (a) $N_{agg} = 30$, (b) $N_{agg} = 41$, and (c) $N_{agg} = 53$. The small ions are omitted for clarity.

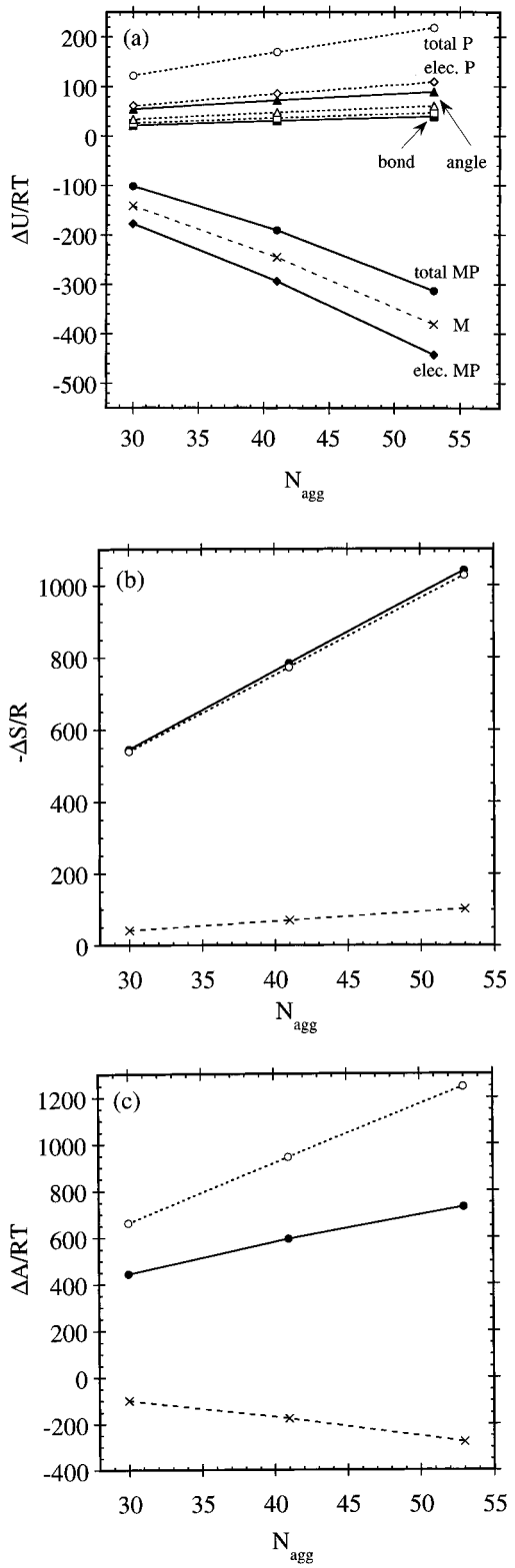

Figure 5. (a) Difference in total energy (ΔU) and its components (ΔU_{elec}, ΔU_{bond}, and ΔU_{angle}), (b) difference in entropy (ΔS), and (c) difference in free energy (ΔA) between the coupled and decoupled M system (dashed curves), P system (dashed curves), and MP system (solid curves) as a function of micellar aggregation numbers (N_{agg}). The ordinate is in reduced unit per system. The largest estimated uncertainties are $\sigma(\Delta U/RT) = 0.5$, $\sigma(\Delta S/R) = 0.55$, and $\sigma(\Delta A/RT) = 0.25$.

differences in entropy and free energy for the M, P, and MP systems are given Figure 5, b and c, respectively, where ΔA is evaluated according to eq 2 and ΔS from the difference between ΔU and ΔA.

Figure 5a shows that ΔU_M is negative for all micellar aggregation numbers and that ΔU_M as well as $\Delta U_M/N_{agg}$ decreases with N_{agg}. The entropy change for the coupling process for the M system is small relative to those for the P and MP systems (Figure 5b), since only the electrostatic interactions are affected. The quantity $-\Delta S_M/N_{agg}$ increases as the aggregation number of the micelles becomes larger. The main contribution to the increase in $-\Delta S_M/N_{agg}$ is the more uneven radial distribution of the small ions. In Figure 5c we see that ΔA_M becomes negative due to the large energetic contribution and that ΔA_M as well as $\Delta A_M/N_{agg}$ decreases with increasing N_{agg}.

For the P systems, all energy contributions are positive, thus making ΔU_P positive. They also increase with the number of beads, and $\Delta U_P/n_{bead}RT$ increases slightly from ca. 2.71 to 2.75 as n_{bead} is raised from 45 to 80 ($n_{bead} = 1.5N_{agg}$). The largest contribution to ΔU_P comes from the electrostatic interaction, followed by the angular and bond energy. The P system displays a large negative entropy change, which originates from the confinements of the beads into a chain and the accumulation of the counterions close to the polyelectrolyte as the coupling is turned on. Moreover, $-\Delta S_P/n_{bead}$ is increased with increasing number of polyelectrolyte beads. Since both ΔU_P and $-\Delta S_P$ are positive and increase with N_{agg}, ΔA_P is consequently positive and increases with increasing number of beads. The increase in ΔA_P with N_{agg} is largely dominated by the entropy.

Regarding the MP system, the major dependence of ΔU_{MP} and its components on N_{agg} is the same as for the P system. The main difference occurs in the electrostatic energy, which is ca. $240RT-540RT$ lower for the MP system due to the favorable electrostatic interaction between the micelle and the polyelectrolyte. This favorable electrostatic interaction causes (i) a more repulsive angular energy, ca. 30−40 higher for the MP system because of the folding of the polyelectrolyte around the micelle, and (ii) a less repulsive bond energy of the polyelectrolyte. The former is in agreement with a smaller persistence and statistic Kuhn segment lengths and the latter with an average bead−bead separation closer to the equilibrium value (cf. Table 3). Both these conformational changes facilitate the possibility for the polyelectrolyte to increase its favorable electrostatic interaction with the micelle. The MP system displays very similar entropy difference and dependency on the number of surfactants (or beads) as compared with the P system. The difference between the P and MP systems amounts to ca. $5.5R$ for $N_{agg} = 30$ (0.18 per surfactant) and increases to ca. $14.2R$ for $N_{agg} = 53$ (0.27 per surfactant), where the MP system has the lower entropy. Finally, we arrive to the free energy given in Figure 5c. The ΔA_{MP} (of forming the micelle−polyelectrolyte complex from a neutral micelle and neutral and nonbonded beads; see Figure 1) is positive since the entropy cost dominates over the gain in energy. As the polyelectrolyte becomes longer and the micelle larger, $\Delta A_{MP}/N_{agg}$ decreases since the N_{agg} dependency on $\Delta U_P/N_{agg}$ is larger than that on $\Delta S_{MP}/N_{agg}$.

Now the change in the thermodynamic quantities for the full mixing process of the micellar and the polyelectrolyte solutions, as described in Figure 1, can be calculated (see part 1 for details). Figure 6 shows that this mixing is energetically as well as entropically favored, making ΔA_{pe} strongly negative. The major contribution to the favorable mixing free energy comes from the energy, but the relative importance of the entropy contribution increases with increasing N_{agg}.

To summarize, and as also stated in parts 1 and 2, the negative mixing free energy for the complexation process given in Figure 1 originates from the attractive micelle−polyelectrolyte electrostatic interaction. This interaction leads to (i) a large reduction of the electrostatic energy for the complexation process and (ii) an increase in entropy by the release of the small ions

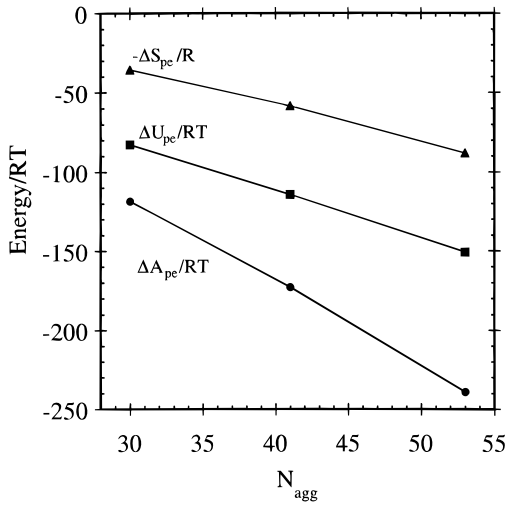

Figure 6. Change in energy (ΔU_{pe}), entropy (ΔS_{pe}), and free energy (ΔA_{pe}) for the mixing process given in Figure 1 as a function of micellar aggregation number (N_{agg}). The ordinate is in reduced unit per system. The largest estimated uncertainties of $\Delta U/RT$, $\Delta U/RT$, and $\Delta A/RT$ are $\sigma(\Delta U/RT) = 0.7$, $\sigma(\Delta U/RT) = 0.75$, and $\sigma(\Delta A/RT) = 0.3$, respectively.

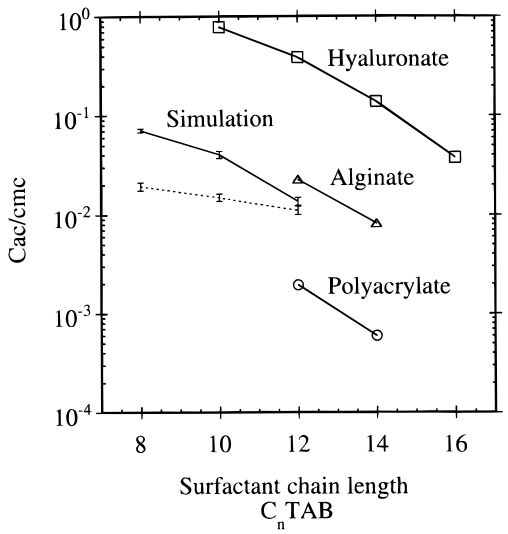

Figure 7. Simulated (dashed and solid curves with error bars) and experimental cac/cmc ratios in the presence of different anionic polyelectrolytes for alkyltrimethylammonium bromides (C_nTAB) as a function of the number of alkyl carbon atoms. The dashed curve denotes simulated data without and the solid one simulated data with corrections for free surfactants and finite volume (see text). The error bars denote the 95% confidence limit using Student's *t*-distribution with nine degrees of freedom and $\sigma(\Delta A_{pe})$ evaluated as described in the section Method and Model System. The experimental polyelectrolyte concentrations and temperatures are 50 mM hyaluronate at 25 °C, 1.0 mM alginate at 30 °C, and 0.5 mM fully carboxylated polyacrylate at 30 °C, and the data are taken from ref 13 (hyaluronate) and ref 12 (alginate and polyacrylate).

accumulated close to the micelle and the polyelectrolyte. Thus, the micelle−polyelectrolyte complexation is energetically and entropically favored, and both contributions grow (also as counted per surfactant) as the micellar charge increases at constant surface charge density. Finally, we notice that the change in the mixing entropy of the counterions of the surfactants in the micelle−polyelectrolyte mixing process is relevant for the consideration of the cac/cmc ratio. But, of course, the change of the mixing entropy of these ions is much smaller (nearly zero) for the real physical process of forming a micelle−polyelectrolyte complex from polyelectrolytes and dispersed surfactants, since the small ions are similarly distributed in the solution before and after this process.

Comparison with Experiments. As previously described, the micellar radii and charges of the three different micelles we selected to correspond to what are found for micelles formed by C_8TAB, $C_{10}TAB$, and $C_{12}TAB$ (cf. Table 1). Most experiments with C_nTAB have been made for $n = 12-14$, but simulations of a micelle formed by $C_{14}TA^+$ surfactants were too time-consuming. From the calculated change in the mixing free energy, ΔA_{pe}, we can estimate the reduction of the cmc due to the presence of the polyelectrolyte according to eq 1. Figure 7 (dashed curve) shows the cac/cmc ratio as a function of the micellar aggregation number.

Before making the comparison between simulated and experimental data, we will consider the effects of neglecting the occurrence of free surfactant (zero salt concentration) and the effects from the finite micellar concentrations (the cell model) on the cac/cmc ratio. We have employed the same approach as in parts 1 and 2, i.e., used the Poisson−Boltzmann equation to estimate these contributions. The use of an estimated cmc value of 250 mM for C_8TAB,[20] and cmc values of 63 and 14 mM for $C_{10}TAB$ and $C_{12}TAB$,[29] respectively, gave the free energy corrections of $1.30RT$, $1.00RT$, and $0.21RT$ per surfactant or a change of the cac/cmc ratio by factors of 3.6, 2.7, and 1.2 for micelles formed by C_8TA^+, $C_{10}TA^+$, and $C_{12}TA^+$ surfactants, respectively. The adjusted cac/cmc ratios are also given in Figure 7 (solid curve with error bars). Thus, at the higher cmc's the salt and finite micelle concentration corrections are nonnegligible in comparison to the effect of the complexation as such.

In our model, there are no potential terms representing hydrophobic interactions, i.e., the electrostatic interaction is the *only* driving force for the complexation. Hence, comparison should be made with experimental systems, where the polyelectrolyte is made of hydrophilic segments. In Figure 7, we also include experimental cac/cmc rations for surfactants (C_nTAB) complexed with three different hydrophilic polyelectrolytes: hyaluronate, alginate, and polyacrylate. Some of the experimental conditions are given in the caption of Figure 7. The cac is here operationally defined as the concentration at which the surfactant binding to the polyelectrolyte starts to increase rapidly (Figures 1 and 2 in ref 12 and Figures 7 and 10 in ref 13).

To assess which of the experimental systems our model polyelectrolyte resembles at most, the average linear charge separation and the persistence length of the polyelectrolytes have to be estimated and compared with the values of 8.3 Å and $l_p \approx 60$ Å, respectively, of the model polyelectrolyte. We estimate hyaluronate to have an average linear charge separation of ca. 12 Å, whereas its persistence length has been reported to $l_p \approx 80$ Å.[32] NaCMC [sodium (carboxymethyl)cellulose] has a similar structure to alginate, and a persistence length of $l_p \approx 50$ Å has been reported for NaCMC with a linear charge distance of ca. 8 Å at a polyelectrolyte concentration of ca. 0.2×10^{-3} g/cm^3.[30] Regarding alginate, we estimate it to have an average linear charge separation of 8−10 Å. Moreover, we expect l_p to slightly exceed 50 Å, since alginate has some α-(1→4) bonds, which should stiffen the polyelectrolyte somewhat, whereas NaCMC only contains β-(1→4) bonds between the saccharide groups.[12] At last, the linear charge separation of polyacrylate is estimated to 5−6 Å. Obviously, alginate, as well as NaCMC with a chosen linear charge separation of ca. 8 Å, is closest and in fact corresponds quite well to our model polyelectrolyte, whereas the linear charge separation of hyaluronate is too large and of polyacrylate too small.

In the model we have employed the same micellar aggregation number in the M and MP systems. Experimental results have shown that the surfactant aggregation number undergoes only minor changes (reduction) upon addition of polyacrylate or

highly charged NaCMC (hydrophilic polyelectrolytes),[17] and hence this assumption should be fulfilled.

Figure 7 shows that the cac/cmc ratio decreases as the alkyl chain becomes longer for all three experimental systems, and the same trend is also observed for our model. The calculated cac/cmc ratio corresponding to C_{12}TAB agrees well with the experimental values for alginate, and according to the discussion above, alginate is the polyelectrolyte which is closest to our model one. This is encouraging. Moreover, for C_{12}TAB we estimate a cac/cmc $\approx 2.5 \times 10^{-2}$ with NaCMC from the binding isotherms given in ref 12 (1.0 mM NaCMC with an estimated linear charge separation of ca. 9 Å at 30 °C), also in line with the model results. As the surfactant chain length is reduced, a deviation from a logarithmic behavior is obtained from the model calculations. Such behavior is also observed for hyaluronate with C_nTAB (see Figure 7). Further studies with alginate with C_{12}TAB and/or simulations for C_{14}TAB are probably needed before a more detail discussion of the nonlogarithmic behavior. Nevertheless, it appears that our simple model is able to capture essential experimental data (i) on the magnitude of the cac/cmc ratio and (ii) on the main dependence of the ratio on the surfactant tail length.

Finally, a limiting point in our study is the short polyelectrolyte, 45−80 beads, with a bead−bead separation of ca. 8.3 Å, which corresponds roughly to a molecular mass (g/mol) of 7000−18 000 (e.g., 9000 for sodium alginate) to 12 000−30 000 (e.g., 16 000 for sodium alginate). For the time being, it is computationally too demanding to treat considerably longer polyelectrolyte chains, especially since free energies are computed (which increases the computation 15-fold). However, the chains should still be sufficiently long to account for the main effects of the reduction of the cmc in dilute solutions, which, as we believe, are the favorable electrostatic micelle−polyelectrolyte interaction and the related release of the counterions of the micelle and of the polyelectrolyte. We also notice that, for a more complete description, the effects of the intermicellar interactions and simultaneous complexation of several polyelectrolytes with one micelle have to be addressed.

Conclusion

On the basis of Monte Carlo simulation and thermodynamic integration of model systems containing one charged micelle and polyelectrolyte, we have investigated the effects of the surfactant tail length on the micelle−polyelectrolyte complex and on the changes in thermodynamic quantities for the corresponding complexation. The micelles formed by the different surfactants differ in size but have the same surface charge density.

The cac was found to be up to 2 orders of magnitude lower than the cmc, and the cac/cmc ratio decreases with increasing surfactant tail length. The electrostatic screening by the free surfactants becomes important as the surfactant tail length decreases (larger cac), and for surfactants equal to and smaller than $C_{12}TA^+$ this contribution becomes significant. Both the strong attractive electrostatic interaction between the micelle and the polyelectrolyte and the release of their counterions were found to be important for the reduction of the cmc. As the tail length increases, (i) the decrease in the complexation energy is dominated by the decrease in the electrostatic interaction energy caused by a less curved micellar surface, whereas the changes in angular and bond energies are of opposite sign and smaller in magnitude, and (ii) the release of counterions becomes more important and results in an enhanced increase in entropy. Furthermore, our results clearly show that the surfactant tail length has only a relatively small effect on the main structure of the complex formed.

Thus, still keeping the shortcomings of the model used in mind, we still believe that the present approach is an important step for increasing our understanding of the micelle−polyelectrolyte complexation and its implications on the self-assembly of charged surfactants. The present results together with those in parts 1 and 2 gives a united picture of how the strength of the micelle−polyelectrolyte complex and hence the cac/cmc ratio depends on (i) the flexibility of the polyelectrolyte, (ii) the linear charge density of the polyelectrolyte, and (iii) the surfactant tail length. We also believe that the current approach should be applicable for the examination of the interaction between polyelectrolytes and charged nanoparticles as well as to polyelectrolyte−globular protein interactions. We are presently considering cases where favorable short-range interaction between the surfactants and the polyelectrolyte lead to a penetration of the polyelectrolyte into the micelle with an accompanying reduction of the aggregation number and an even larger reduction of the cmc by using a mean-field lattice approach.

Acknowledgment. We thank Per Hansson for valuable discussions. This work has been supported by grants from the Swedish National Board for Industrial and Technical Development (NUTEK) and the Swedish National Science Research Council (NFR).

References and Notes

(1) Hayakawa, K.; Kwak, J. C. T. *J. Phys. Chem.* **1982**, *86*, 3866.
(2) Santerre, J., P.; Hayakawa, K.; Kwak, J. C. T. *Colloids Surf.* **1985**, *13*, 35.
(3) Abuin, E.; Scaiano, J. P. *J. Am. Chem. Soc.* **1984**, *106*, 6274.
(4) Chu, D.; Thomas, J. K. *J. Am. Chem. Soc.* **1986**, *108*, 6270.
(5) Goddard, E. D. *Colloids Surf.* **1986**, *19*, 301.
(6) Gao, Z.; Kwak, J. C. T.; Wasylishen, R., E. *J. Colloid Interface Sci.* **1988**, *126*, 371.
(7) Skerjanc, S.; Kogej, K.; Vesnaver, G. *J. Phys. Chem.* **1988**, *92*, 6382.
(8) Yingije, L.; Dubin, P. L.; Havel, H. A.; Edwards, S. L.; Dautzenberg, H. *Langmuir* **1995**, *11*, 2486.
(9) Thalberg, K.; Lindman, B.; Karlström, G. *J. Phys. Chem.* **1990**, *94*, 4289.
(10) Wong, T. S.; Thalberg, K.; Lindman, B.; Gracz, H. *J. Phys. Chem.* **1991**, *95*, 8850.
(11) Lindman, B.; Thalberg, K. Polymer-Surfactant Interactions−Recent Developments. In *Interactions of Surfactants with Polymers and Proteins*; Goddard, E. D., Ananthapadmanabhan, K. P., Eds.; CRC Press: Boca Raton, FL, 1993.
(12) Hayakawa, K.; Santerre, J. P.; Kwak, J. C. T. *Macromolecules* **1983**, *16*, 1642.
(13) Thalberg, K.; Lindman, B. *J. Phys. Chem.* **1989**, *93*, 1478.
(14) Thalberg, K.; Lindman, B.; Bergfeldt, K. *Langmuir* **1991**, *7*, 2893.
(15) Kiefer, J.; Somasundaran, P.; Anaanthapadmanabhan, K. P. *Langmuir* **1993**, *9*, 1187.
(16) Hansson, P.; Almgren, M. *Langmuir* **1994**, *10*, 2115.
(17) Hansson, P.; Almgren, M. *J. Phys. Chem.* **1996**, *100*, 9038.
(18) Wallin, T.; Linse, P. *Langmuir* **1996**, *12*, 305.
(19) Wallin, T.; Linse, P. *J. Phys. Chem.* **1996**, *100*, 17873.
(20) Evans, D. F.; Wennerström, H. *The Colloidal Domain*; VCH Publishers: New York, 1994.
(21) Carnahan, N. F.; Starling, K. E. *J. Chem. Phys.* **1969**, *51*, 635.
(22) Hansen, J. P.; McDonald, I. R. *Theory of Simple Liquids*; Academic Press: London, 1976.
(23) Linse, P. *J. Phys. Chem.* **1986**, *90*, 6821.
(24) Tanford, C. *J. Phys. Chem.* **1972**, *76*, 3020.
(25) Magny, B.; Iliopoulos, I.; Zana, R.; Audebert, R. *Langmuir* **1994**, *10*, 3180.
(26) Roelants, E.; De Schryver, F. C. *Langmuir* **1987**, *3*, 209.
(27) Allen, M. P.; Tildesley, D. J. *Computer Simulations of Liquids*; Clarendon Press: Oxford, 1987.
(28) Madras, N.; Sokal, A. D. *J. Stat. Phys.* **1988**, *50*, 109.
(29) van Os, N. M.; Haak, J. R.; Rupert, L. A. M. *Physico-Chemical Properties of Selected Anionic, Cationic and Nonionic Surfactants*; Elsevier Science Publishers B. V.: Amsterdam, 1993.
(30) Moan, M.; Wolf, C. *Polymer* **1975**, *16*, 776.
(31) Flory, P. J. *Statistical Mechanics of Chain Molecules*, Interscience: New York, 1969.
(32) Fouissac, E.; Milas, M.; Rinaudo, M.; Borsali, R. *Macromolecules* **1992**, *25*, 5613.